CHEMISTRY OF MATERIALS

ARTICLE

pubs.acs.org/cm

Poly(*N*-isopropylacrylamide)-Coated Superparamagnetic Iron Oxide Nanoparticles: Relaxometric and Fluorescence Behavior Correlate to Temperature-Dependent Aggregation

Sharavanan Balasubramaniam,[†] Nikorn Pothayee,[†,‡] Yinnian Lin,[†,‡] Mike House,[⊥] Robert C. Woodward,[⊥] Timothy G. St. Pierre,[⊥] Richey M. Davis,[*,§,†] and J. S. Riffle[†,‡]

[†]Macromolecules and Interfaces Institute, [‡]Department of Chemistry, and [§]Department of Chemical Engineering, Virginia Tech, Blacksburg, Virginia 24061, United States

[⊥]School of Physics, The University of Western Australia, Crawley, Western Australia 6009, Australia

ABSTRACT: Magnetic nanoparticles coated with polymers have existing and further potential for applications in medicine, including magnetic resonance imaging (MRI) imaging for diagnostics and assessing biodistribution, and their capacity to remotely generate heat in response to alternating current magnetic fields to elicit biological responses. Advances in such domains rely on developing better understanding of how such materials respond to magnetic fields. This paper reports thermosensitive properties of poly(*N*-isopropylacrylamide-*co*-Nile Red)-coated magnetic nanostructures upon passing through the lower critical solution temperature (LCST) of the polymer brush, and correlation of this behavior with formation of aggregates. Discrete magnetite nanoparticles coated with brush layers comprised of terminally attached poly(*N*-isopropylacrylamide-*co*-Nile Red) afforded highly water-dispersible nanoparticles (intensity average diameter of 38 nm) with good colloidal stability in phosphate buffers. The nanoparticles displayed enhanced transverse (T_2) NMR relaxometric behavior as the temperature was increased through the LCST. Moreover, incorporation of the environmentally sensitive Nile Red dye into the copolymer leads to significant changes in fluorescence emission intensity upon aggregation that present new possibilities for the remote fluorescence detection of aggregated structures.

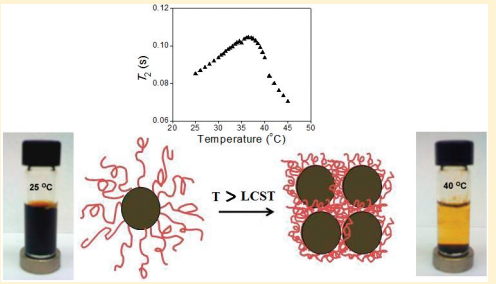

KEYWORDS: contrast agents, magnetite, poly(*N*-isopropylacrylamide), T_2, LCST, thermally responsive, Nile Red

INTRODUCTION

Superparamagnetic iron oxide nanoparticles have a range of existing and potential biomedical applications such as contrast agents for magnetic resonance imaging (MRI), hyperthermia treatment of cancer, tags for cell separations, retinal detachment therapy, and targeted drug delivery.[1−9] Magnetite (Fe_3O_4) has attracted much attention, because of its superior magnetic properties combined with stability, biocompatibility, and low cytotoxicity.[10] The development of MRI as a versatile imaging modality has provided a major thrust to the design and optimization of colloidal iron oxide nanoparticles, which belong to the class of T_2 contrast agents. The contrast-enhancing characteristics of magnetite nanoparticles have been attributed to a microscopic susceptibility effect, whereby dephasing of the diffusing water protons is accelerated by field gradients created by the induced magnetization of the particles. However, the degree of contrast enhancement, defined by the transverse relaxivity coefficient (r_2), depends on various parameters such as particle size, magnetization and aggregation, and interrelationships among chemical and physical parameters of the nanoparticles and relaxivities have not been well-defined.

Recently, it has been shown that aggregates of magnetic nanoparticles in suspension can cause a greater reduction in T_2 than the primary nanoparticles ($T_2 = 1/R_2$).[11−13] This decrease in T_2 on aggregation can be related to either an increase in average particle size within the *motional-averaging regime*, where T_2 is proportional to $1/r^2$ or with a larger fraction of the particle size distribution being located within the *static-dephasing regime*, where R_2 has its maximum value and is independent of r. If the aggregates grow too large, then T_2 will eventually increase as the system moves into the *echo-limited regime*, where T_2 is proportional to r^2.[13−16]

The higher proton relaxation rates translate to better contrast in T_2-weighted magnetic resonance images. As a result, some effort has now turned toward creating controlled clusters of magnetic nanoparticles. Berret et al.[17] have described the controlled clustering of maghemite (γ-Fe_2O_3) nanoparticles through electrostatic complexation with cationic−non-ionic block copolymers. They reported enhanced transverse relaxivities for the clusters, compared to primary nanoparticles, and also observed an increase in r_2 with increases in the size of the clusters. Gao et al. reported very high transverse relaxivities of clusters of oleic acid-coated magnetite nanoparticles encased in hydrophobic cores of poly(ε-caprolactone-*b*-ethylene oxide) micelles in water.[18]

Received: March 30, 2011
Revised: May 27, 2011
Published: June 21, 2011

dx.doi.org/10.1021/cm2009048 | *Chem. Mater.* 2011, 23, 3348–3356

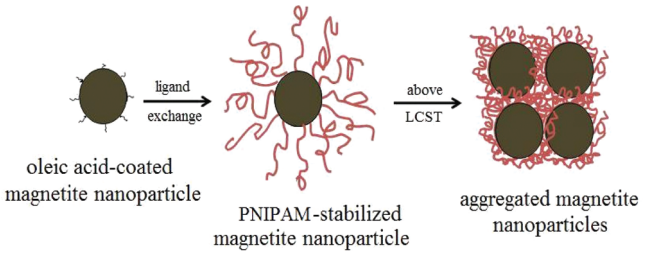

Figure 1. Lower critical solution temperature (LCST)-induced aggregation in water of individually coated magnetite−PNIPAM nanoparticles.

Previous data from our laboratories haves also shown that small clusters of individually coated poly(ethylene oxide)-magnetite complexes can form in water when sufficiently low polymer loadings are utilized, and that these also correlate with enhanced r_2.[19]

Modulation of T_2 relaxation times by reversible aggregation of magnetic nanoparticles has also been demonstrated. Osborne et al.[20] have reported "smart" T_2 contrast agents based on dextran sulfate-coated iron oxide nanoparticles derivatized with a light-sensitive molecule (spiropyran). Conformational switching of the latter between hydrophilic and hydrophobic isomers, in response to light irradiation, resulted in reversible aggregation of the nanoparticles with an ∼33% difference in the T_2 relaxation times of the dispersed nanoparticles and the aggregates. Weissleder and co-workers[21] developed an *in vitro* MRI probe that employs cross-linked iron oxide nanoparticles functionalized with DNA sequences. Upon recognition of a complementary oligonucleotide, the nanoparticles aggregate into clusters leading to reduced T_2 relaxation times. The process was reversible through the action of a DNA-cleaving enzyme that separated the clusters into the constituent nanoparticles. Schellenberger et al.[22] have described protease-specific T_2 contrast agents comprised of peptide−poly(ethylene oxide) copolymers adsorbed on citrate-coated iron oxide nanoparticles. The action of matrix metalloproteinase 9 led to cleavage of the peptide-poly(ethylene oxide) copolymer, resulting in irreversible aggregation and higher r_2.

Poly(*N*-isopropylacrylamide) (PNIPAM) has been one of the most studied water-soluble polymers, ever since its lower critical solution temperature (LCST) behavior was first described by Heskins and Guillet.[23] Above the LCST (∼32 °C), PNIPAM chains in aqueous solution undergo a phase transition from an expanded coil to a collapsed state, as a result of loss of hydration. We have recently reported the synthesis of magnetic nanostructures where a bis(phosphonate)-functional PNIPAM was terminally attached to discrete magnetite nanoparticles.[24] Herein, we report thermoresponsive core−shell nanoparticles comprised of ∼8-nm-diameter magnetite stabilized in water by a PNIPAM-*co*-Nile Red corona, with temperature-dependent aggregation and NMR relaxation effects. We describe the LCST-induced aggregation and the effect on T_2 shortening of highly water-dispersible magnetite−PNIPAM nanoparticles (see Figure 1). When heated above the LCST of PNIPAM in water, the nanoparticles aggregated because of a loss of steric stabilization. However, the state of dispersion could be fully restored by cooling the suspension down to ambient temperature and sonicating. The LCST-induced aggregation of the magnetite-PNIPAM nanoparticles was observed using a combination of dynamic light scattering, steady-state fluorescence spectroscopy and magnetic resonance relaxometry. Thermally driven aggregation of magnetite-PNIPAM complexes has been studied previously;[3,25−27] however, until now, the effect of this aggregation on the relaxometric properties has not been studied. For the fluorescence experiments, *N*-isopropylacrylamide was copolymerized with an acrylate monomer containing Nile Red, and the copolymer was adsorbed onto the magnetite to render the nanoparticles fluorescent. Changes in the transverse and longitudinal relaxation times of water protons were investigated as a function of aggregation of the nanoparticles. The nature of the environment of the Nile Red co-monomer in the hydrated (nonaggregated) versus dehydrated (aggregated) state was accompanied by a significant change in fluorescence intensity, thus providing an additional means of detecting the onset of dehydration and aggregation.

EXPERIMENTAL SECTION

Materials. All materials were used as received unless otherwise noted. Benzyl alcohol (>98%), diethyl ether, diethyl vinyl phosphonate (97%), hexanes (HPLC grade), iron(III) acetylacetonate ($Fe(acac)_3$), trimethylsilyl bromide (TMSBr, 97%), oleic acid (90%, technical grade), 2-chloropropionyl chloride, 3-amino-1-propanol, diethylaminophenol (97%), sodium nitrite (>97%), 1,6-dihydroxynaphthalene (99%), thallium ethoxide (98%), and acryloyl chloride (97%) were purchased from Aldrich. *N*-isopropylacrylamide (NIPAM) was recrystallized twice from hexane. Tris[2-(dimethylamino)ethylamine] (Me_6TREN) was synthesized and purified according to a previously reported method.[28] Dichloromethane (anhydrous), acetone (HPLC grade), concentrated HCl (ACS plus), ethyl acetate (99.9%) and isopropanol (USP) were purchased from Fisher Scientific. Ethanol (200 proof) was purchased from Decon Laboratories. Dialysis tubing (25 000 and 3500 g mol^{-1} MWCO) was obtained from Spectra/Por. Phosphate buffered saline (PBS) was obtained from Mediatech. A NdFeB permanent magnet with a diameter of $^{11}/_{16}$ in. and a thickness of $^{1}/_{4}$ in. was obtained from K and J Magnetics. It was axially magnetized with a surface field of 3880 G.

Synthesis of Oleic Acid-Coated Magnetite Nanoparticles. Magnetite nanoparticles were synthesized using a method that was slightly modified from that previously reported.[18,19] $Fe(acac)_3$ (2.14 g, 8.4 mmol) and benzyl alcohol (45 mL, 0.43 mol) were charged to a 250-mL, three-neck, round-bottom flask equipped with a water condenser and nitrogen inlet and placed in a Belmont metal bath with an overhead stirrer with thermostatic (±1 °C) control. The solution was held at 110 °C for 1 h under N_2; the temperature was then increased to 205 °C and maintained for 40 h. The reaction was cooled to room temperature and the particles were collected by centrifugation (4000 rpm, 30 min). The magnetite nanoparticles were washed three times with acetone (100 mL each), then they were dispersed in chloroform (20 mL) containing oleic acid (0.3 g). The solvent was removed under vacuum at room temperature, and the oleic acid-coated magnetite nanoparticles were washed three times with acetone (100 mL each) to remove excess oleic acid. The particles were dried under vacuum for 24 h at 25 °C.

Synthesis of Nile Red Acrylate. *(5-Diethylamino)-2-Nitrosophenol Hydrochloride.* 3-Diethylaminophenol (16.5 g, 0.1 mol) was dissolved in a mixture of 35 mL of concentrated HCl and 20 mL of water and cooled to 0 °C. A solution of sodium nitrite (6.9 g, 0.1 mol) in 50 mL of water was added dropwise over 2 h, and the temperature of the reaction was maintained at 0−5 °C. The resulting brown slurry was stirred for 3.5 h. Following filtration and washing with 30 mL of 4 M aqueous HCl, the product was dried, then recrystallized from 150 mL of ethanol to yield a yellow powder (16.4 g, 72%). ^{1}H NMR in DMSO-d_6: δ = 7.36 (1H, d), 6.90 (1H, d), 5.74 (1H, s), 3.60 (4H, m), 1.20 (6H, t).

9-Diethylamino-2-hydroxy-5H-benzo[α]phenoxazin-5-one (NR-OH). 2-Hydroxy-substituted-Nile Red (NR−OH) was synthesized via a known procedure, according to Briggs et al.[29] 5-Diethylamino-2-nitrosophenol

dx.doi.org/10.1021/cm2009048 |*Chem. Mater.* 2011, 23, 3348–3356

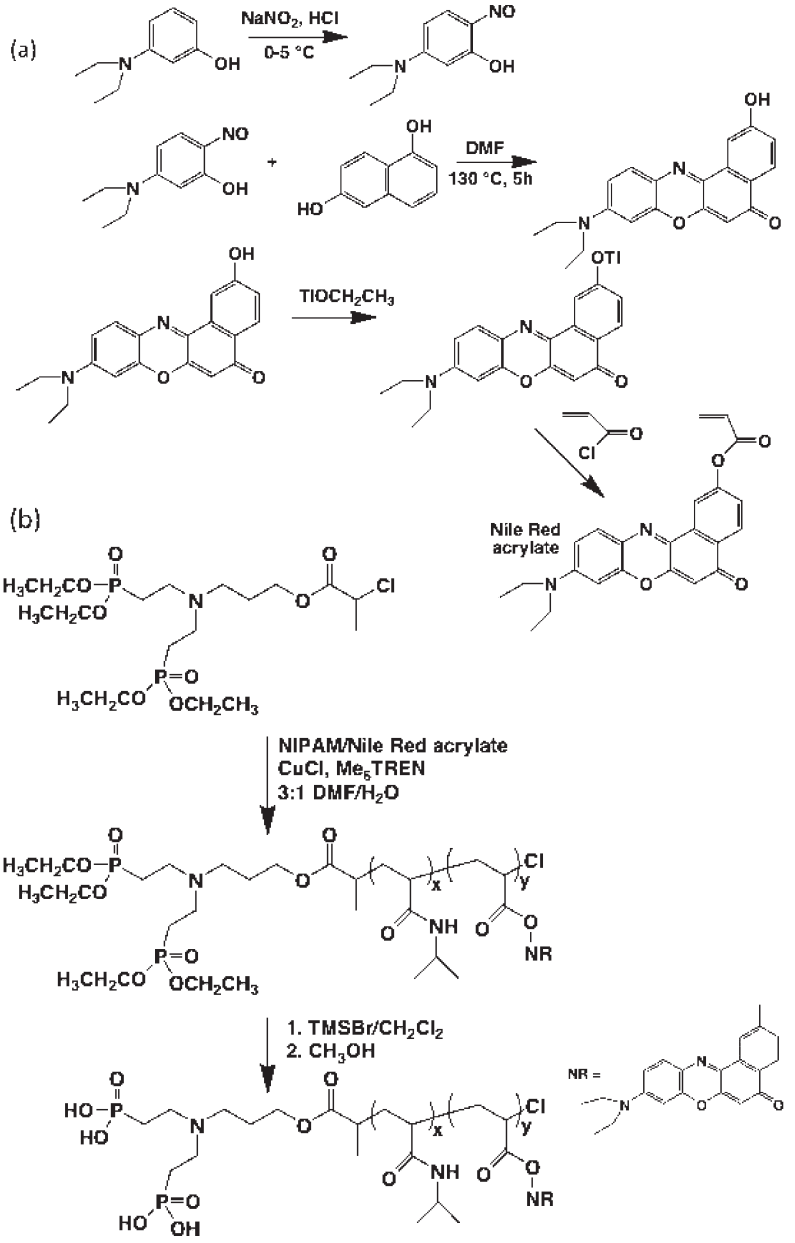

Figure 2. (a) Synthesis of a Nile Red-containing acrylate monomer; (b) synthesis of bis(phosphonate) functional PNIPAM-*co*-Nile Red acrylate.

hydrochloride (1.28 g, 5.5 mmol) and 1,6-dihydroxynaphthalene (0.90 g, 5.6 mmol) were dissolved in 250 mL of dry DMF and heated under reflux for 5 h. The solvent was removed under reduced pressure to yield a dark blue-green solid. Subsequent purification by silica gel column chromatography (ethyl acetate:isopropanol, 4:1) yielded 0.52 g (28%) of a dark green solid. ^{1}H NMR in DMSO-d_6: δ = 10.38 (1H, s), 7.94 (1H, d), 7.86 (1H, d), 7.56 (1H, d), 7.07 (1H, dd), 6.78 (1H, d), 6.62 (1H, d), 6.13 (1H, s), 3.48 (4H, q), 1.17 (6H, t).

Acrylate Monomer Containing Nile Red (NR-acrylate). A Nile Red acrylate monomer was prepared in a two-step procedure that included treatment of NR-OH with thallium ethoxide in a solvent to form the thallium salt (NR-OTl), then NR-OTl was reacted with acryloyl chloride to yield the NR-acrylate monomer. Thallium ethoxide (0.15 mL, 2.12 mmol) was added to a solution of NR-OH (0.42 g, 1.26 mmol) in 30 mL of dry DMF, and the mixture was stirred at room temperature for 2 h. Then, 0.34 mL of acryloyl chloride (4.20 mmol) was added into the reaction mixture and stirred overnight. To remove the thallium salt formed in the reaction, the mixture was passed through a small silica gel column and then the column was washed with ethyl acetate. Evaporation of the solvents in the eluent yielded 0.48 g (1.24 mmol, 98% yield) of a NR-acrylate monomer. ^{1}H NMR in DMSO-d_6: δ = 8.26 (1H, s), 8.17 (1H, d), 7.61 (1H, d), 7.51 (1H, d), 6.84 (1H, d), 6.67 (1H, s), 6.61 (1H, d), 6.46 (1H, dd), 6.28 (1H, s), 6.21 (1H, d), 3.48 (4H, q), 1.17 (6H, t).

Synthesis of Ammonium Bis(phosphonate)-Functional PNIPAM and Bis(Phosphonate)-Functional Poly(NIPAM-co-Nile Red Acrylate). Bis(phosphonate)-PNIPAM and bis(phosphonate)-PNIPAM-*co*-Nile Red acrylate were synthesized by a procedure adapted from our previous work.[24] A bis(phosphonate)-functional ATRP initiator (Figure 2) was prepared and utilized with CuCl/Me_6TREN as a catalyst system for the polymerizations. The initiator (0.32 g, 6.48 $\times$ 10^{-4} mol), NIPAM (4.6 g, 4.07 $\times$ 10^{-2} mol), CuCl (65 mg, 6.48 $\times$ 10^{-4} mol), Me_6TREN (190 μL, 6.48 $\times$ 10^{-2} mol), and a DMF:H_2O mixture (v:v 3:1, 8 mL) were added to a 25-mL Schlenk flask. After it was degassed by three freeze−pump−thaw cycles, the flask was kept under a slight pressure of N_2.

dx.doi.org/10.1021/cm2009048 |*Chem. Mater.* 2011, 23, 3348–3356

The reaction mixture was immersed in an oil bath at 25 °C for polymerization. After 60 min, the mixture was diluted with THF (20 mL) and passed through an alumina column to remove the copper catalyst. The polymer was isolated by precipitation in *n*-hexane twice, collected by filtration, and dried under vacuum at room temperature for 24 h. The number-average molecular weight (M_n) determined by size-exclusion chromatography (SEC) was ~11 000 g mol^{-1} with a polydispersity index (PDI) of 1.07. ^{1}H NMR revealed that there were ~65 NIPAM repeat units per initiator moiety. To remove the ethoxy groups from the (bis)phosphonate end group, bis(phosphonate)-PNIPAM (1.10 g, 1.53×10^{-4} mol) was dissolved in anhydrous dichloromethane (30 mL). Trimethylsilyl bromide (0.190 g, 1.22×10^{-3} mol) was added dropwise to the mixture under a dry N_2 atmosphere. The solution was stirred at room temperature for 24 h; then, most of the solvent and byproduct was removed under vacuum at room temperature. Anhydrous methanol (5 mL) was added to the resultant polymer and stirred for 4 h. Bis(phosphonic acid)-PNIPAM was recovered by precipitation into hexane and dried under vacuum. Bis(phosphonate)-PNIPAM-*co*-Nile Red acrylate was synthesized in a similar procedure using a 50:1 molar ratio of NIPAM to the Nile Red acrylate. To remove any unreacted free monomer, the polymer (1 g) was dissolved in methanol (5 mL) and dialyzed twice against methanol (2 L) through a cellulose acetate membrane (MWCO, 3500 g mol^{-1}). The co-polymer was recovered by precipitation into hexane, then dried under vacuum at room temperature.

Coating of Magnetite Nanoparticles with PNIPAM and PNIPAM-*co*-Nile Red Acrylate. A representative method for preparing PNIPAM-coated magnetite nanoparticles with a targeted composition of 33 wt % magnetite is provided. Oleic acid-coated magnetite nanoparticles (33.0 mg) were dispersed in chloroform (10 mL) and charged into a 50-mL round-bottom flask. A polymer blend of ammonium bis(phosphonate)-functional PNIPAM and PNIPAM-*co*-Nile Red acrylate (50:50 wt %, 67.0 mg) was dissolved in DMF (10 mL) and added to the dispersion. The reaction mixture was sonicated in a VWR Model 75T sonicator for 4 h under N_2 and then stirred at room temperature for 24 h. The nanoparticles were precipitated in hexanes (300 mL). A permanent magnet was utilized to collect the magnetite nanoparticles and free oleic acid was decanted with the supernatant. The particles were dried under vacuum at room temperature overnight, then dispersed in deionized water (20 mL) with sonication for 30−60 s. The complex was dialyzed against deionized water (1 L) for 24 h using a 25 000 g mol^{-1} MWCO dialysis bag, then freeze-dried to obtain a "purple-brown" solid product.

CHARACTERIZATION

^{1}H NMR spectra of the polymers were acquired at 400 MHz (Varian Unity or Varian INOVA). SEC analysis was performed on a liquid chromatograph that was equipped with a Waters Model 1515 isocratic HPLC pump, Waters Autosampler, Waters Model 2414 refractive index detector, and Viscotek Model 270 RALLS/viscometric dual detector. The mobile phase was *N*-methylpyrrolidone that contained 0.05 M LiBr. A Waters Styragel HR-1 + HR-3 + HR-4 column set maintained at 60 °C, because of the viscous nature of NMP, was used. Both the solvent and the sample solution were filtered before introduction into the SEC system. Absolute molecular weights were determined with a Universal Calibration that was based on polystyrene standards.

Inductively coupled plasma−atomic emission spectroscopy (ICP-AES) was performed on a SPECTRO Model ARCOS 165 ICP spectrometer (SPECTRO Analytical Instruments, Germany) to measure the concentration of iron in the magnetite-polymer complexes. The particles (10 mg) were dispersed in deionized water (5 mL). The dispersion (1 mL) was mixed with 4 mL of concentrated nitric acid to digest magnetite and release free iron. The mixture was reacted for 5 days at room temperature and diluted with deionized water to a concentration of 0.02 mg mL^{-1} prior to measurement. The reported results are the mean of three measurements.

Dynamic light scattering (DLS) measurements were performed using a Zetasizer NanoZS particle analyzer (Malvern Instruments Ltd., Malvern, U.K.) equipped with a 4-mW solid-state He−Ne laser (λ = 633 nm) at a scattering angle of 173°. The average translational diffusion coefficient (D_t) was extracted from a single exponential (cumulants) fit of the correlation curve and the intensity-average hydrodynamic diameter (D_I) was determined through the Stokes−Einstein equation:

$$D_I = \frac{k_B T}{3\pi\eta D_t} \quad (1)$$

where k_B is the Boltzmann constant, T the absolute temperature, and η the solvent viscosity. Samples dispersed in deionized water to appropriate concentrations were passed through a 100-nm syringe filter (Whatman Anotop) before measurements. The reported intensity-weighted hydrodynamic diameters were averaged from three measurements.

Fluorescence measurements were performed on a Model Synergy Mx multimode microplate reader (BioTek Instruments, Winooski, VT) at an excitation wavelength of 570 nm. Samples were equilibrated at 25 and 35 °C for 15 min, and the fluorescence emission was recorded from 600 nm to 850 nm.

Transmission electron microscopy (TEM) was performed on a Philips Model EM-420 field-emission-gun TEM system operating at an acceleration voltage of 100 kV. Samples were prepared by casting a drop of a dilute aqueous solution of PNIPAM-stabilized magnetite nanoparticles onto an amorphous carbon-coated copper grid. Images were acquired at a magnification of 96 000×, corresponding to a resolution of 3.88 pixels nm^{-1}. The sizes of over 2000 particles from different regions of the grid were measured using Reindeer Graphics' Fovea Pro 4 plug-in for Adobe Photoshop 7.0.

The sample magnetization (M), as a function of the applied field (H) (the $M-H$ curve) was measured at 300 K, using a superconducting quantum interference device (SQuID) magnetometer (MPMS XL, Quantum Design) in the range of ±7 T. In addition, a zero-field-cooled/field-cooled (ZFC/FC) test[16] was conducted using the SQuID magnetometer to confirm that the sample was superparamagnetic at room temperature and to determine the maximum blocking temperature.

Magnetic resonance relaxometry was performed with a Model mq-60 NMR Analyzer (Bruker Minispec) operating at a magnetic field of 1.4 T. This field strength corresponds to a proton Larmor frequency of 60 MHz. Proton transverse relaxation times (T_2) were obtained from fitting a monoexponential decay curve to signal data generated by a Carr−Purcell−Meiboom−Gill (CPMG) spin−echo pulse sequence with an echo spacing of 1 ms and a repetition time of 5 s. Longitudinal relaxation times (T_1) were obtained from fitting a monoexponential recovery curve to signal data generated with an inversion recovery (IR) pulse sequence using 10 logarithmically spaced inversion times between 50 ms and 10 000 ms. Each sample (500 μL) was transferred into a 7.5-mm NMR tube and equilibrated at each temperature for 15 min prior to measurements.

RESULTS AND DISCUSSION

The polymers for these complexes were synthesized by controlled radical polymerizations, wherein the ligands for adsorption

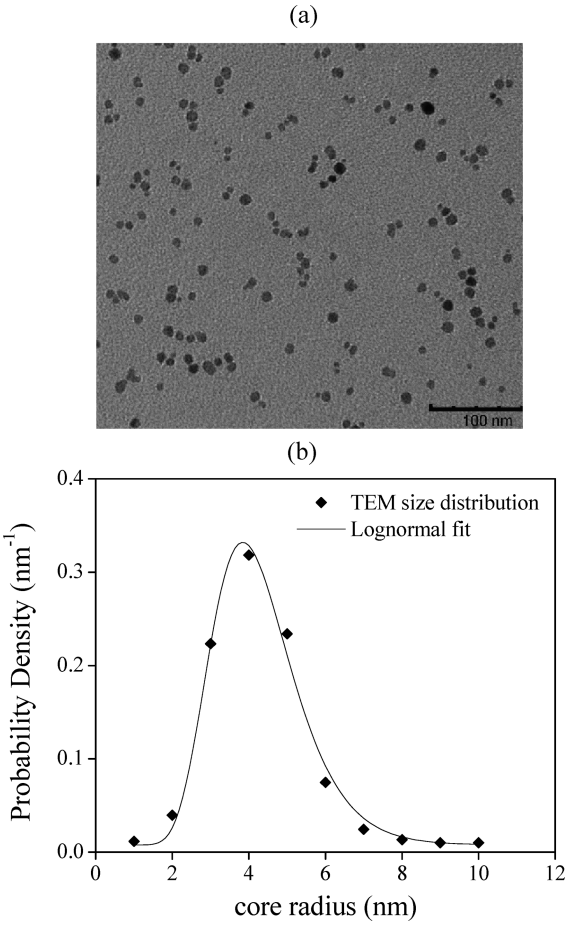

Figure 3. (a) Representative TEM image of PNIPAM-coated magnetite nanoparticles. (b) The observed TEM particle sizes were described by a log-normal distribution function (continuous line) to yield an average radius of 4.14 ± 1.52 nm.

onto the magnetite surfaces were incorporated in the initiators (see Figure 2).[24] Thus, they were designed to adsorb onto the particles from one end only, to provide well-defined brushes that are comprised of terminally attached chains. This was done to minimize any aggregation of the particles due to multiple adsorption sites on the polymers during the coating process. The ATRP polymerization of bis(phosphonate)-functional PNIPAM and PNIPAM-*co*-Nile Red acrylate, followed by their adsorption onto discrete magnetite nanoparticles from organic media, afforded magnetite-PNIPAM complexes. The final composition of the complexes was determined by ICP-AES analysis to be 65.1 ± 0.26 wt % polymer, which was in good agreement with the targeted composition of 67 wt %. This result was also consistent with previous findings in our group that phosphonate-functional polymers can be adsorbed onto magnetite in high concentrations.[30,31]

Figure 3a shows a representative TEM image of the PNIPAM-coated magnetite nanoparticles. Only the magnetite cores are distinguishable, because of their relatively high electron density. The sizes of ~2400 particles were measured and the data were fitted by the log-normal distribution function:

$$P(r) = \frac{1}{\sqrt{2\pi}\sigma r} \exp\left\{\frac{-[\ln(r/r_m)]^2}{2\sigma^2}\right\} \qquad (2)$$

where $P(r)$ is the probability density of the distribution, r the core radius, r_m the median radius, and σ^2 the variance. The median radius of the magnetite nanoparticles was 4.14 nm, and the standard deviation was 1.52 nm.

The hydrodynamic sizes of the magnetite−PNIPAM complexes were estimated using a modified density distribution model originally developed for star polymers to account for the polymer brush layer and using the core size distribution to account for the polydispersity of the magnetite.[32] This modified model has been used in our group to predict the sizes of magnetite−polymer complexes, wherein the magnetite nanoparticles were stabilized with polyether brushes in water and polydimethylsiloxane brushes in chloroform, to within 8% without any adjustable parameters.[31,33,34] Comparison of the predicted sizes with the hydrodynamic diameters measured experimentally by DLS allowed us to determine whether the magnetite−PNIPAM complexes consisted mostly of dispersed primary particles or of aggregates. Based on the average number of chains per particle and the solution properties of PNIPAM in water at 25 °C (number of statistical segments, 21.7; length of each statistical segment, 1.34 nm; and the Flory exponent, 0.518),[35,36] the intensity-average diameter D_I of the complexes was estimated to be 36 nm. The value of D_I obtained from DLS was 38 nm. The agreement between the predicted and measured hydrodynamic sizes indicates that the complexes consisted mostly of individually dispersed nanoparticles. The relatively narrow size distribution of the complexes was also evident from the low PDI values (<0.15) obtained from dynamic laser scattering (DLS).

The ZFC/FC curves for the magnetite−PNIPAM complexes are shown in Figure 4a, which shows that the sample is superparamagnetic at 300 K with a maximum blocking temperature of 140 K. The magnetization (M) versus applied field (H) curve for the magnetite−PNIPAM complexes at 300 K is depicted in Figure 4b. The magnetite−PNIPAM complex has a saturation magnetization (M_S) of 17.5 emu per gram of polymer−iron oxide complex at an applied field of 20 kOe. Since the complex consists of 35 wt % iron oxide, this corresponds to a room-temperature M_S value of ~50 emu g^{-1} for the iron oxide nanoparticle core. The decrease in saturation magnetization, compared to the value of bulk magnetite, can be attributed to spin canting caused by reduced coordination and broken exchange at the particle surface and/or broken symmetry associated with crystalline disorder.[37−40]

Thermally induced aggregation of the magnetite−PNIPAM complexes in water was characterized by DLS. Figure 5 shows the evolution of hydrodynamic size of the nanoparticles in water (0.1 mg mL^{-1}), as a function of temperature. The intensity-weighted diameter was recorded at each temperature, because of its sensitivity to aggregation arising from the sixth-power dependence of the scattering intensity on radius.[41] At 25 °C, the complexes exhibited a constant diameter (D_I = 38 nm). As the temperature was increased above ~33.5 °C, the hydrodynamic size increased, signaling the onset of aggregation induced by passing through the LCST. Below the LCST, the PNIPAM chains are hydrated random coils that extend into solution. The highly expanded and mutually repulsive chains are effective in providing steric stabilization to the nanoparticle dispersions and preventing aggregation due to attractive van der Waals forces and magnetic dipolar interactions. When heated above the transition temperature, a thermodynamically driven phase separation occurs, which is characterized by increased contact between the

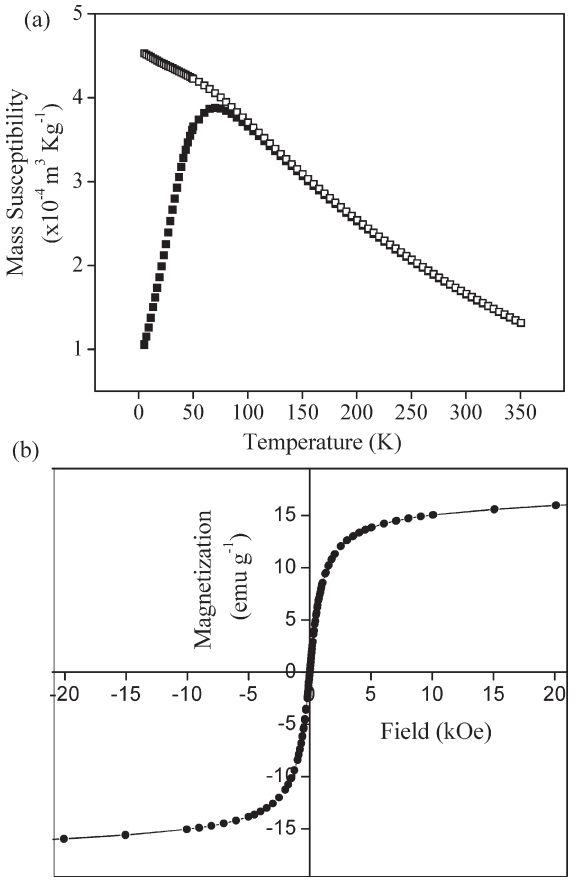

Figure 4. (a) ZFC/FC curves of magnetite−PNIPAM nanoparticles at H = 100 Oe, showing superparamagnetic behavior at 300 K (■ = ZFC; □ = FC). (b) Magnetization versus applied field (hysteresis) curve of magnetite−PNIPAM nanoparticles at 300 K. The saturation magnetization is 17.5 emu per gram of iron oxide-PNIPAM complex.

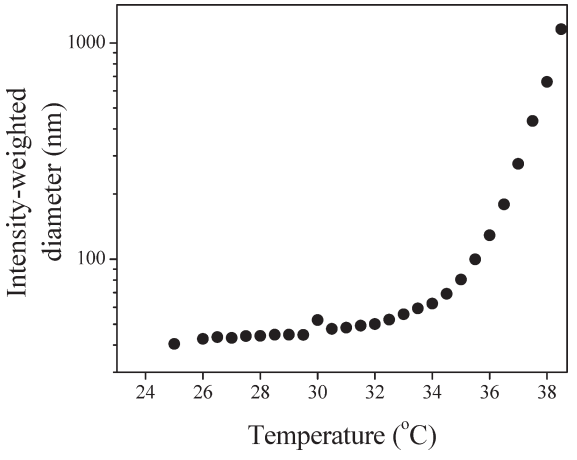

Figure 5. Evolution of hydrodynamic size of magnetite−PNIPAM as a function of temperature by DLS.

polymer segments accompanied by a loss of hydration.[42,43] At the transition temperature, the interaction between the polymer chains changes from net repulsion to net attraction.[44] This results in aggregate formation in the dispersion in the absence of steric stabilization, which is evident as a continuous increase in the hydrodynamic size.

Aggregation of the complexes above the LCST of the polymer was probed by steady-state fluorescence spectroscopy of the magnetite−PNIPAM nanoparticles containing the Nile Red-acrylate co-monomer in the brush layers. An acrylate derivative of the highly fluorescent laser dye, Nile Red, was copolymerized with NIPAM to form a bis(phosphonate)-functional PNIPAM-*co*-Nile Red copolymer; then, this co-polymer was adsorbed onto the magnetite nanoparticles through the bis(phosphonate) end group to form a brush layer. The fluorescence of PNIPAM-*co*-Nile Red-coated nanoparticles in aqueous solution was markedly red-shifted, with respect to emission in relatively nonpolar solvents with a maximum emission intensity at λ = 665 nm. The solvatochromic behavior of Nile Red has been well-studied, and the dye has been used by many researchers as a hydrophobic probe, because of its remarkable sensitivity to the polarity of the microenvironment.[45−49] At 25 °C in water, there was no difference in fluorescence emission wavelengths between a PNIPAM-*co*-Nile Red copolymer solution and the magnetite-PNIPAM-*co*-Nile Red nanoparticles. At 35 °C, which is above the LCST transition of PNIPAM-*co*-Nile Red, we observed a remarkable quenching of the fluorescence of the magnetite−polymer complex (Figure 6b). Such fluorescence quenching is characteristic of aggregated, planar conjugated chromophores such as Nile Red.[50,51] In aqueous solution, the fluorescence of Nile Red is normally quenched, since it aggregates, because of its hydrophobic nature. It is reasoned that covalently incorporating the Nile Red co-monomer in the hydrophilic PNIPAM chain prevents the dye from aggregating below the LCST and that this results in the observed fluorescence from the magnetite−PNIPAM-*co*-Nile Red complexes in water at 25 °C (see Figure 6a). It is reasoned that flocculation of the magnetite−PNIPAM-*co*-Nile Red nanoparticles above the LCST of the polymer led to concomitant dye aggregation and fluorescence quenching (see Figure 6b).

NMR relaxometry performed on dispersions of the magnetite−PNIPAM complexes, as a function of temperature, also revealed dramatic shortening of T_2 relaxation times above the LCST transition temperature of PNIPAM. Figure 7a shows the results for complexes at concentrations of 0.05 and 0.1 mg mL^{-1}. For relatively small particles, the transverse relaxation time of solutions of these particles can be represented by the *motional-averaging regime* described by eq 3:

$$\frac{1}{T_2} = \frac{16f(\Delta\omega)^2 r^2}{45D} \qquad (3)$$

where f is the volume fraction occupied by the magnetic particles in solution, $\Delta\omega$ the spread of Larmor frequencies at the surface of the particle, r the particle/cluster radius, and D the self-diffusion coefficient of water.[12]

Below the LCST of PNIPAM, where the complexes are individually dispersed nanoparticles, the trend is governed by the temperature dependence of the self-diffusion coefficient of water. The gradual increase in D with temperature causes a concomitant increase in T_2, according to eq 2. However, the T_2 was observed to peak at ~35 °C, and this was followed by a sharp and continuous decrease with temperature. This was attributed to the LCST-induced aggregation of complexes causing significant relaxation rate $(1/T_2)$ enhancement. The agglomerated nanoparticles, because of their larger size, have longer correlation

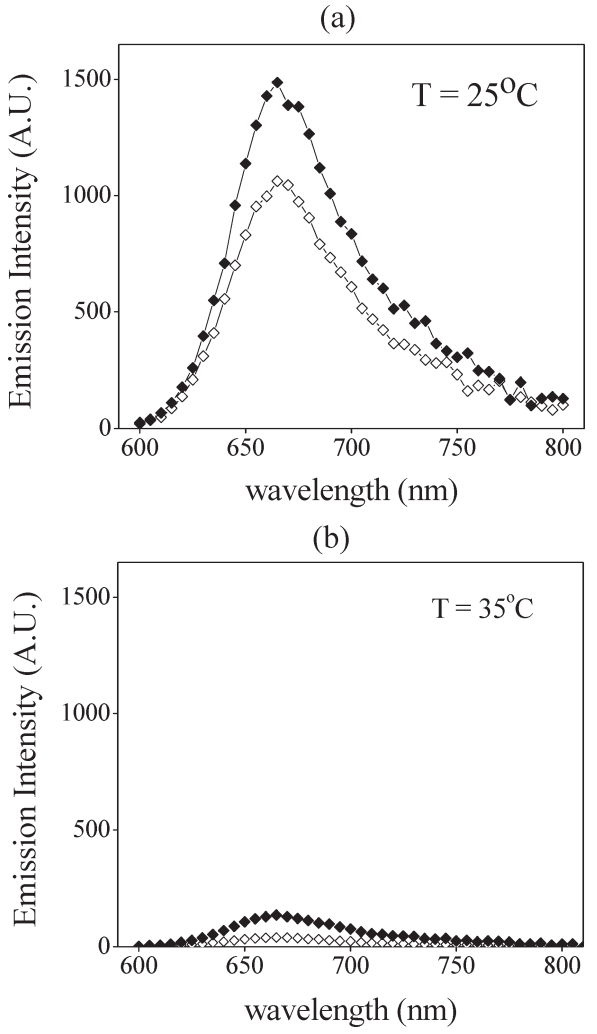

Figure 6. (a) Fluorescence of magnetite−PNIPAM-*co*-Nile Red nanoparticles below LCST. (b) Fluorescence quenching due to aggregation of nanoparticles above the LCST. Data are shown for concentrations of (◆) 0.1 mg mL^{-1} and (◇) 0.05 mg mL^{-1}.

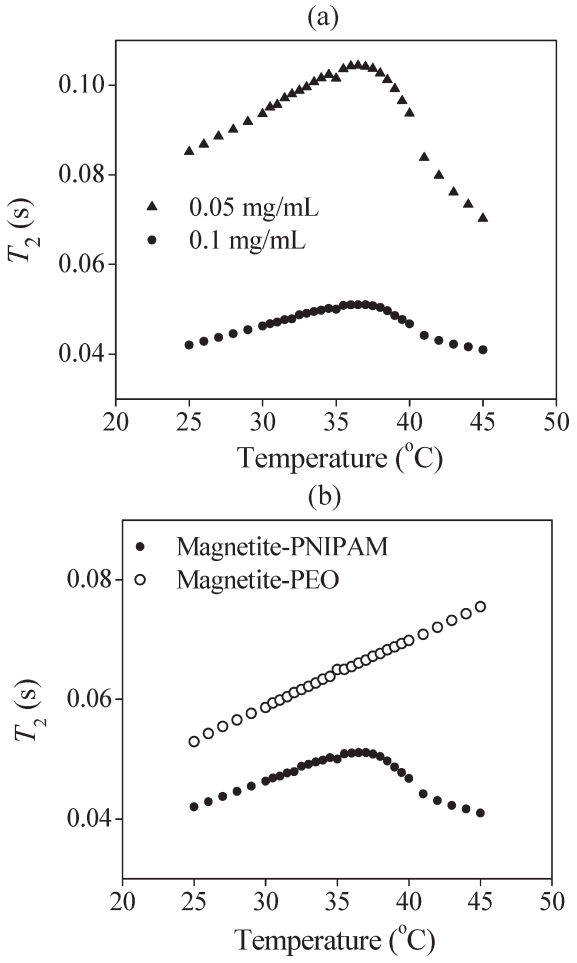

Figure 7. (a) LCST-induced aggregation of magnetite−PNIPAM nanoparticles leads to shortening of the T_2 relaxation times. Data shown are for (▲) 0.05 mg mL^{-1} and (●) 0.1 mg mL^{-1} of complexes in deionized water. (b) Comparison of T_2 relaxation times of (●) magnetite−PNIPAM and (○) magnetite−PEO nanoparticles at a concentration of 0.1 mg mL^{-1}.

times (time = r^2/D) and shorter T_2 relaxation times. A control experiment was performed with poly(ethylene oxide)-coated magnetite nanoparticles under the same experimental conditions. These complexes were similar to the PNIPAM-coated magnetite described in this paper: the polymer loading was 67% and the polymer was anchored to the magnetite using terminal phosphonate moieties. The detailed synthesis and characterization of the magnetite−PEO complexes is described elsewhere.[30,31] As shown in Figure 7b, the variation of T_2 of the PEO-coated magnetite, unlike the case of PNIPAM-coated nanoparticles, was entirely linear in the range of temperatures studied, reflecting only changes in the self-diffusion coefficient of the water. This confirms that the LCST-induced aggregation of primary magnetite−PNIPAM nanoparticles was indeed responsible for the observed reduction of T_2 relaxation times.

According to Roch et al.,[12] the formation of aggregates leads to reduction in the exchange of fast-relaxing water protons within the aggregate with the slow-relaxing protons in the bulk water outside the aggregate, thus increasing T_1. Any enhanced hydrophobicity of the polymer above the LCST may also inhibit direct access of water protons to the magnetic particles, which could also increase T_1 relaxation times. This behavior was observed with the magnetite−PNIPAM complex above the LCST (Figure 8). As in the case for T_2 relaxation, the control magnetite−PEO complex did not show any noticeable change in the T_1 relaxation times over the range of 25−45 °C.

Figure 9 illustrates the temperature/magnetic field dual responsivity of the magnetite−PNIPAM nanoparticles. At 25 °C (less than LCST), the particles were highly dispersible in water and exhibited good colloidal stability at concentrations as high as 20 mg mL^{-1}. No sedimentation was observed when a vial containing the dispersion was placed atop a NdFeB permanent magnet. By contrast, at 40 °C (>LSCT), there was a sharp increase in turbidity and the particles could be collected with the permanent magnet. The ability to collect the particles with a magnet is due to an increase in the magnetophoretic mobility as the particles aggregate above the LCST. For the same field and field-gradient conditions, the magnetophoretic mobility increases with the square of the radius. The dispersibility of the complexes could be fully restored by cooling the dispersions to room temperature and sonicating. This experiment provided further confirmatory evidence that the thermoresponsive nature of the PNIPAM shell triggered aggregation of the nanoparticles.

dx.doi.org/10.1021/cm2009048 |*Chem. Mater.* 2011, 23, 3348–3356

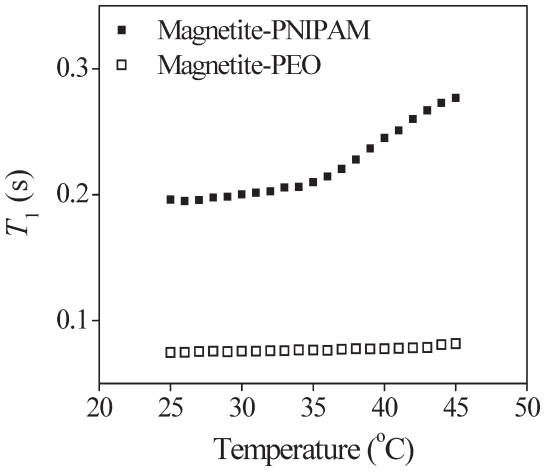

Figure 8. (■) Effect of aggregation of magnetite−PNIPAM nanoparticles on the T_1 relaxation time. (□) Behavior of equivalent magnetite−PEO nanoparticles (shown for the sake of comparison).

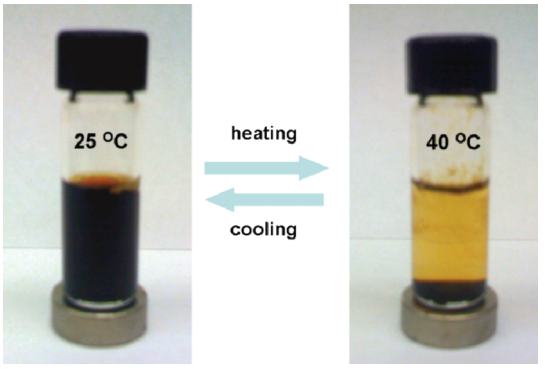

Figure 9. Dispersion−flocculation behavior of magnetite−PNIPAM nanoparticles, as a function of temperature and magnetic field (concentration = 20 mg mL^{-1}).

We envisage that both temperature and magnetic-field sensitivity offer potential for the design of "smart" multifunctional magnetic nanocarriers for biomedical applications, such as drug delivery combined with the capability to monitor biodistribution through magnetic resonance imaging (MRI). We believe that the ability to conjugate Nile Red in the brush layers, as demonstrated in this work, lends the thermoresponsive magnetite−PNIPAM-*co*-Nile Red nanoparticles to investigations of localized heating effects under the influence of an external alternating-current (AC) magnetic field by monitoring changes in fluorescence. Localized temperature increases in the brush, which are caused by orientational relaxation processes in the superparamagnetic nanoparticle cores, can be harnessed to potentially release biologically active molecules held in the brush through noncovalent forces.[52,53] Current efforts by our group also include detailed investigations on the thermally induced aggregation behavior of these nanoparticles with an objective to fabricate controlled magnetic nanoclusters for enhanced performance as T_2 contrast agents.

CONCLUSIONS

We have reported on the thermoresponsive properties of magnetite core-PNIPAM-*co*-Nile Red shell nanoparticles. Well-defined, water-dispersible nanostructures were synthesized via atom transfer radical polymerization of bis(phosphonate)-terminated PNIPAM-*co*-Nile Red acrylate followed by adsorption of the polymer onto discrete magnetite nanoparticles. The temperature-dependent aggregation of nanoparticles induced by the lower critical solution temperature (LCST) of the PNIPAM-*co*-Nile Red shell was observed by dynamic light scattering (DLS), fluorescence spectroscopy, and nuclear magnetic resonance (NMR) relaxometry. Aggregation was accompanied by drastic shortening of the transverse relaxation times. In addition, the fluorescence emission derived from the Nile Red acrylate co-monomer being dispersed in water below the LCST was quenched dramatically upon aggregation of the co-polymer above the LCST. Combining a thermosensitive polymeric shell with a magnetic core paves the way for multi-stimuli-responsive nanoparticles, such as "smart" T_2 contrast agents for magnetic resonance imaging (MRI) or materials that induce a biological response because of changes in brush structure around the magnetic core.

AUTHOR INFORMATION

Corresponding Author

*Address: 130 Randolph Hall, Department of Chemical Engineering, Virginia Tech, Blacksburg, VA 24061. Tel.: (540) 231-4578. E-mail: rmdavis@vt.edu.

ACKNOWLEDGMENT

The authors gratefully acknowledge the support of the National Science Foundation (under Contract Nos. DMR 0909065 and DMR 0805179) and the Australian Research Council's Discovery Projects funding scheme (Project No. DP0985848).

REFERENCES

(1) Bulte, J. W. M.; Kraitchman, D. L. *NMR Biomed.* **2004**, *17*, 484–499.
(2) Lee, H.; Lee, E.; Kim, D. K.; Jang, N. K.; Jeong, Y. Y.; Jon, S. *J. Am. Chem. Soc.* **2006**, *128*, 7383–7389.
(3) Regmi, R.; Bhattarai, S. R.; Sudakar, C.; Wani, A. S.; Cunningham, R.; Vaishnava, P. P.; Naik, R.; Oupicky, D.; Lawes, G. *J. Mater. Chem.* **2010**, *20*, 6158–6163.
(4) Mefford, O. T.; Woodward, R. C.; Goff, J. D.; Vadala, T. P.; St Pierre, T. G.; Dailey, J. P.; Riffle, J. S. *J. Magn. Magn. Mater.* **2007**, *311*, 347–353.
(5) Wilson, K. S.; Goff, J. D.; Riffle, J. S.; Harris, L. A.; St Pierre, T. G. *Polym. Adv. Technol.* **2005**, *16*, 200–211.
(6) Jain, T. K.; Morales, M. A.; Sahoo, S. K.; Leslie-Pelecky, D. L.; Labhasetwar, V. *Mol. Pharm.* **2005**, *2*, 194–205.
(7) Purushotham, S.; Ramanujan, R. V. *J. Appl. Phys.* **2010**, *107*, 114701-1–9.
(8) Krishnan, K. M. *IEEE Trans. Magn.* **2010**, *46*, 2523–2558.
(9) Latorre, M.; Rinaldi, C. *P. R. Health Sci. J.* **2009**, *28*, 227–238.
(10) Weissleder, R.; Bogdanov, A.; Neuwelt, E. A.; Papisov, M. *Adv. Drug Delivery Rev.* **1995**, *16*, 321–334.
(11) Matsumoto, Y.; Jasanoff, A. *Magn. Reson. Imaging* **2008**, *26*, 994–998.
(12) Roch, A.; Gossuin, Y.; Muller, R. N.; Gillis, P. *J. Magn. Magn. Mater.* **2005**, *293*, 532–539.
(13) Carroll, M. R. J.; Woodward, R. C.; House, M. J.; Teoh, W. Y.; Amal, R.; Hanley, T. L.; St Pierre, T. G. *Nanotechnology* **2010**, *21*, No. 035103.
(14) Gillis, P.; Moiny, F.; Brooks, R. A. *Magn. Reson. Med.* **2002**, *47*, 257–263.

(15) Yablonskiy, D. A.; Haacke, E. M. *Magn. Reson. Med.* **1994**, *32*, 749–763.
(16) Bedanta, S.; Kleemann, W. *J. Phys. D* **2009**, *42*, 013001-1–28.
(17) Berret, J. F.; Schonbeck, N.; Gazeau, F.; El Kharrat, D.; Sandre, O.; Vacher, A.; Airiau, M. *J. Am. Chem. Soc.* **2006**, *128*, 1755–1761.
(18) Ai, H.; Flask, C.; Weinberg, B.; Shuai, X.; Pagel, M. D.; Farrell, D.; Duerk, J.; Gao, J. M. *Adv. Mater.* **2005**, *17*, 1949–1952.
(19) Carroll, M. R. J.; Huffstetler, P. P.; Miles, W. C.; Goff, J. D.; Davis, R. M.; Riffle, J. S.; House, M.; Woodward, R. C.; Pierre, T. G. S. Unpublished work.
(20) Osborne, E. A.; Jarrett, B. R.; Tu, C. Q.; Louie, A. Y. *J. Am. Chem. Soc.* **2010**, *132*, 5934−5935.
(21) Perez, J. M.; Josephson, L.; O'Loughlin, T.; Hogemann, D.; Weissleder, R. *Nat. Biotechnol.* **2002**, *20*, 816–820.
(22) Schellenberger, E.; Rudloff, F.; Warmuth, C.; Taupitz, M.; Hamm, B.; Schnorr, J. *Bioconjugate Chem.* **2008**, *19*, 2440–2445.
(23) Heskins, M.; Guillet, J. E. *J. Macromol. Sci. A: Pure Appl. Chem.* **1968**, *2*, 1441–1455.
(24) Pothayee, N.; Balasubramaniam, S.; Davis, R. M.; Riffle, J. S.; Carroll, M. R. J.; Woodward, R. C.; Pierre, T. G. S. *Polymer* **2011**, *52*, 1356–1366.
(25) Rubio-Retama, J.; Zafeiropoulos, N. E.; Serafinelli, C.; Rojas-Reyna, R.; Voit, B.; Cabarcos, E. L.; Stamm, M. *Langmuir* **2007**, *23*, 10280–10285.
(26) Herrera, A. P.; Rodriguez, M.; Torres-Lugo, M.; Rinaldi, C. *J. Mater. Chem.* **2008**, *18*, 855–858.
(27) Herrera, A. P.; Barrera, C.; Zayas, Y.; Rinaldi, C. *J. Colloid Interface Sci.* **2010**, *342*, 540–549.
(28) Xia, J. H.; Gaynor, S. G.; Matyjaszewski, K. *Macromolecules* **1998**, *31*, 5958–5959.
(29) Briggs, M. S. J.; Bruce, I.; Miller, J. N.; Moody, C. J.; Simmonds, A. C.; Swann, E. *J. Chem. Soc.—Perkin Trans. 1* **1997**, 1051–1058.
(30) Goff, J. D.; Huffstetler, P. P.; Miles, W. C.; Pothayee, N.; Reinholz, C. M.; Ball, S.; Davis, R. M.; Riffle, J. S. *Chem. Mater.* **2009**, *21*, 4784–4795.
(31) Miles, W. C.; Goff, J. D.; Huffstetler, P. P.; Reinholz, C. M.; Pothayee, N.; Caba, B. L.; Boyd, J. S.; Davis, R. A.; Riffle, J. S. *Langmuir* **2009**, *25*, 803–813.
(32) Vagberg, L. J. M.; Cogan, K. A.; Gast, A. P. *Macromolecules* **1991**, *24*, 1670–1677.
(33) Miles, W. C.; Goff, J. D.; Huffstetler, P. P.; Mefford, O. T.; Riffle, J. S.; Davis, R. M. *Polymer* **2010**, *51*, 482–491.
(34) Mefford, O. T.; Carroll, M. R. J.; Vadala, M. L.; Goff, J. D.; Mejia-Ariza, R.; Saunders, M.; Woodward, R. C.; St. Pierre, T. G.; Davis, R. M.; Riffle, J. S. *Chem. Mater.* **2008**, *20*, 2184–2191.
(35) Fang, Z.; Zhen, T.; Sato, T. *Sci. China, Ser. B: Chem.* **1999**, *42*, 290–297.
(36) Hirotsu, S. *J. Chem. Phys.* **1991**, *94*, 3949–3957.
(37) Li, D.; Teoh, W. Y.; Woodward, R. C.; Cashion, J. D.; Selomulya, C.; Amal, R. *J. Phys. Chem. C* **2009**, *113*, 12040–12047.
(38) Morup, S. *J. Magn. Magn. Mater.* **2003**, *266*, 110–118.
(39) Kodama, R. H.; Berkowitz, A. E.; McNiff, E. J.; Foner, S. *Phys. Rev. Lett.* **1996**, *77*, 394–397.
(40) Morales, M. P.; Veintemillas-Verdaguer, S.; Montero, M. I.; Serna, C. J.; Roig, A.; Casas, L.; Martinez, B.; Sandiumenge, F. *Chem. Mater.* **1999**, *11*, 3058–3064.
(41) Berne, B. J.; Pecora, R. *Dynamic Light Scattering: With Applications to Chemistry, Biology, and Physics*; Wiley: New York, 1976.
(42) Schild, H. G. *Prog. Polym. Sci.* **1992**, *17*, 163–249.
(43) Pelton, R. *J. Colloid Interface Sci.* **2010**, *348*, 673–674.
(44) Hunter, R. J.; White, L. R. *Foundations of Colloid Science*; Clarendon Press, and Oxford University Press: Oxford [Oxfordshire], U.K., and New York, 1987.
(45) Greenspan, P.; Fowler, S. D. *J. Lipid Res.* **1985**, *26*, 781–789.
(46) Dutta, A. K.; Kamada, K.; Ohta, K. *J. Photochem. Photobiol. A: Chem.* **1996**, *93*, 57–64.
(47) Tajalli, H.; Gilani, A. G.; Zakerhamidi, M. S.; Tajalli, P. *Dyes Pigments* **2008**, *78*, 15–24.
(48) Vauthey, E. *Chem. Phys. Lett.* **1993**, *216*, 530–536.
(49) Daban, J. R.; Samso, M.; Bartolome, S. *Anal. Biochem.* **1991**, *199*, 162–168.
(50) Levitsky, I.; Krivoshlykov, S. G.; Grate, J. W. *Anal. Chem.* **2001**, *73*, 3441–3448.
(51) deSilva, A. P.; Gunaratne, H. Q. N.; Gunnlaugsson, T.; Huxley, A. J. M.; McCoy, C. P.; Rademacher, J. T.; Rice, T. E. *Chem. Rev.* **1997**, *97*, 1515–1566.
(52) Rahimi, M.; Wadajkar, A.; Subramanian, K.; Yousef, M.; Cui, W. N.; Hsieh, J. T.; Nguyen, K. T. *Nanomedicine* **2010**, *6*, 672–680.
(53) Hoare, T.; Santamaria, J.; Goya, G. F.; Irusta, S.; Lin, D.; Lau, S.; Padera, R.; Langer, R.; Kohane, D. S. *Nano Lett.* **2009**, *9*, 3651–3657.